Interaction of spanwise vortices with a boundary layer

Alan Luton, Saad Ragab, and Demetri Telionis

Citation: Physics of Fluids (1994-present) **7**, 2757 (1995); doi: 10.1063/1.868654
View online: http://dx.doi.org/10.1063/1.868654
View Table of Contents: http://scitation.aip.org/content/aip/journal/pof2/7/11?ver=pdfcov
Published by the AIP Publishing

Interaction of spanwise vortices with a boundary layer

Alan Luton, Saad Ragab,[a] and Demetri Telionis
Department of Engineering Science and Mechanics, Virginia Polytechnic Institute and State University, Blacksburg, Virginia 24061

(Received 19 August 1994; accepted 1 August 1995)

The interaction of a spanwise vortex with a boundary layer has been numerically simulated using a fractional-step method. The incompressible Navier-Stokes equations are solved to accurately predict the strong viscous–inviscid interaction between a vortex either near or embedded within a boundary layer of comparable size. A strong vortex induces an eruption and the production of a secondary vortex. The secondary vortex causes the primary vortex to rebound, a response observed in many previous experiments and numerical simulations. However, weaker vortices as well do not follow the inviscid trajectory despite the absence of a secondary vortex. Rather than creating vorticity at the wall, a weaker vortex mainly redistributes the vorticity of the boundary layer, pulling it away from the wall. The redistributed vorticity alters the path of the vortex. In the laminar cases studied the decay of the vortex is not significantly altered by the boundary layer. © *1995 American Institute of Physics.*

I. INTRODUCTION

The passage of convected vortical structures near a solid body is an important phenomenon in many engineering applications. For instance, in helicopter aerodynamics the wakes from upstream blades can interact with blades downstream, possibly leading to undesirable vibrations.[1,2] Similar phenomena can occur in turbomachines. In separating flows, vortical structures can form which later interact with the solid surface downstream of reattachment.[3] These vortical structures can induce secondary separation and pressure fluctuations along the solid surface. Conversely, a vortex deeply embedded within a boundary layer can be quickly destroyed. Motivation for the study of vortex/wall interactions also stems from interest in the bursting phenomenon in turbulent boundary layers. It is commonly thought that coherent vortical structures passing near the wall can induce eruptions (see, for example, Robinson[4]). The study of vortex induced eruptions in laminar flow could lead to insights into the regeneration process of turbulent boundary layers. A recent review of vortex/wall interactions can be found in Doligalski.[5]

There are many studies which focus on either vortex rings or pairs impinging on a wall in an otherwise stagnant fluid. Typically the vortex is observed to rebound from the wall. The rebound phenomenon was first shown by Harvey and Perry[6] who experimentally studied the motion of a single wing tip vortex near a moving wall. They attributed the upward movement of the primary vortex to the creation of a secondary vortex of opposite sense at the wall. The secondary vortex induces an upward motion to the primary vortex. In their numerical simulations, Peace and Riley[7] demonstrated the rebounding phenomenon of a vortex pair from no-slip and free-slip boundaries. Orlandi,[8] who performed simulations at higher Reynolds number, observed the formation of secondary and tertiary vortices. In a subsequent study Orlandi and Verzicco[9] observed the multiple formation of vortices for the case of an axisymmetric vortex ring. These features have been observed experimentally by Boldes and Ferreri,[10] Walker *et al.*,[11] and others. Similar features are seen for a forced jet impinging on a wall.[12]

There are relatively few investigations of a spanwise vortex interacting with a boundary layer. Nelson *et al.*[13] experimentally studied a vortex generated within the turbulent boundary layer. This was accomplished by lifting from the wall a spoiler whose chordlength is comparable to the boundary-layer thickness. The vortex that forms behind the spoiler is convected downstream but disappears within a few chordlengths. Here we study cases with similar vortex core to boundary-layer thickness ratios.

Numerical studies of spanwise vortices have focused on the solution of the boundary layer equations. Chuang and Conlisk[14] and Peridier *et al.*[15] studied the case of a vortex above a wall with no freestream. Their calculations, based on interacting-boundary-layer methods, show the formation of a secondary eddy and the breakdown of the calculations at a singularity. The singularity indicates there is strong viscous–inviscid interaction in the flow and signals the onset of separation. These methods are not valid for multiple rebounds of the vortex. Their main value lies in the high Reynolds number regime where direct numerical simulations are difficult.

In the current study we consider the case of a convected spanwise vortex in close proximity to a boundary layer. The full two-dimensional, unsteady, incompressible Navier-Stokes equations are solved. In section II the numerical scheme is outlined, including code validation as well as initial and boundary conditions. The results are presented in section III while the conclusions are discussed in section IV.

II. METHOD OF SOLUTION

The incompressible Navier-Stokes equations are given by

$$\frac{\partial u_i}{\partial t}+\frac{\partial}{\partial x_j}u_iu_j=-\frac{\partial p}{\partial x_i}+\frac{1}{Re}\frac{\partial}{\partial x_j}\frac{\partial}{\partial x_j}u_i, \tag{1}$$

[a]Corresponding author: tel: (540) 231-5950; e-mail: ragab@ragab1.esm.vt.edu

$$\frac{\partial u_i}{\partial x_i}=0 \tag{2}$$

where all variables have been nondimensionalized by a characteristic velocity and length. The equations are solved by a scheme first proposed by Kim and Moin[16] and later modified by Le and Moin.[17] The scheme is described in detail in these references so a mere overview is given herein. The scheme consists of a fractional-step (time-splitting) method combined with the approximate factorization technique. The momentum equation is advanced in time in two steps, first applying the convection and diffusion operators and then the pressure operator. Finding the pressure consists of solving Poisson's equation, which is equivalent to satisfying the continuity equation. Solving Poisson's equation is by far the most computationally expensive step. Le and Moin proposed a modification to the Kim and Moin method to increase the CFL while reducing the computational effort. Their scheme employs a three-stage Runge-Kutta scheme in which the convective terms are advanced explicitly and the viscous terms implicitly. The Kim and Moin time splitting is applied at each stage, yet the Le and Moin modification permits Poisson's equation to be solved only at the end of the time step, rather than at each of the three stages. This results in a substantial reduction in the CPU time. In the current work a biconjugate gradient method is used to solve Poisson's equation. The use of a staggered grid facilitates the application of the Neumann boundary condition on the pressure. The right hand side of Poisson's equation is expressible in terms of the velocity field, thus only the velocity needs to be specified on the boundary.

A. Validation of the computer code

Two problems are examined to determine the validity of the computer code: a system of Oseen vortices and the steady flow over a flat plate. The problem of the mutual interaction of a system of vortices is intended to show that the method has little numerical viscosity so that regions of high vorticity are not artificially dissipated. The velocity field of an Oseen vortex is given by

$$v_\theta=\frac{\Gamma}{2\pi r}[1-e^{-r^2/4\nu t}] \tag{3}$$

where v_θ is the tangential velocity, Γ is the circulation, ν is the kinematic viscosity, r is the distance in the radial direction, and t is time. An Oseen vortex is placed at the center of the computational domain which is a square with sides 20 core radii in length. Symmetry conditions are applied at the boundaries which implies an infinite field of vortices, only one of which is modeled. The initial conditions include the effect of vortices outside the boundaries. The Reynolds number based on the circulation at infinity is $Re_\Gamma=2196$. In Fig. 1 the tangential velocity as a function of r is plotted for three different grids at the time when the velocity at $r=r_c$ has decayed by half. The grid sizes are 36×36, 70×70, and 140×140. The grids are stretched in both directions, resulting in 5, 10, and 20 points in the vortex core respectively. The analytic solution is also shown, and consists of the exact solution (given by Eq. 3) with the effect of the closest vortices added in. The numerical solution converges to the known solution as the grid is refined. The center of the vortex experiences no drift, since the velocity at the center remains zero. This indicates that there are no asymmetric errors in the code. Such errors could be introduced by the improper handling of a stretched grid. It is important to confirm that the code does not introduce artificial drift because it is necessary to track the location of the vortex as it convects.

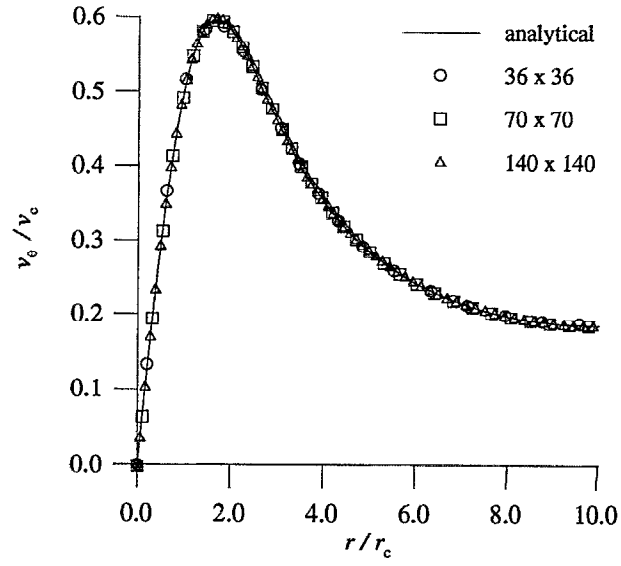

FIG. 1. The tangential velocity of an Oseen vortex as a function of r for three different grids.

The flow over a flat plate has also been computed in order to compare with the Blasius solution. The computational domain extends from $x=0.01$ to $x=0.04$ and $y=0$ to $y=0.004$ where the origin of the axes is at the leading edge of the plate. These values of x correspond to Reynolds numbers of $Re_x=10{,}000$ at the inflow and $Re_x=40{,}000$ at the outflow. A grid of 300×40 was used. A Blasius velocity profile is specified at the inflow and Neumann boundary conditions are applied at the outflow and far-field boundary. In Fig. 2 the u and v velocity profiles are plotted in terms of similarity variables at three different streamwise locations. The agreement is excellent.

B. Initial and boundary conditions

Now consider the initial and boundary conditions for a spanwise vortex convecting near a boundary layer (see Fig. 3). The initial streamwise velocity field has been chosen to be

$$u|_{t=0}=u_{BL}+u_V+u_{VI}+u_{cor} \tag{4}$$

where u_{BL} is the Blasius solution for a flat plate, u_V is the flow field due to an isolated Oseen vortex, u_{VI} is the flow field due to the image vortex, and u_{cor} is a correction to satisfy the no-slip boundary condition. This field is divergence free and satisfies the proper boundary conditions. The no-slip correction is especially desirable for vortices of negative rotation (clockwise) since it reduces the size of the initial separation region below the vortex. Note that the sum of the

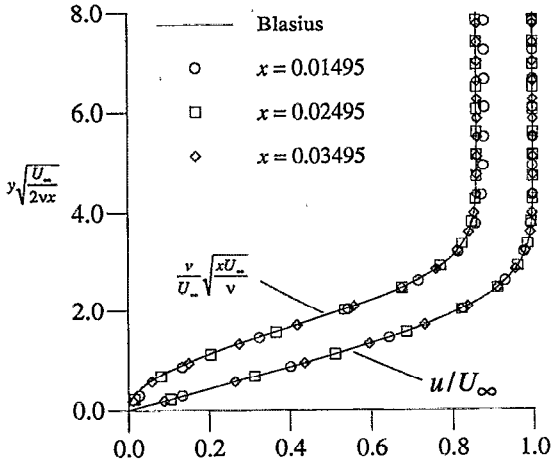

FIG. 2. The velocities at various x locations for flow over a flat plate.

first three terms of the right hand side satisfy the continuity equation and the no-penetration condition, but not the no-slip condition. The correction u_{cor} is related to Rayleigh's impulsively started plate problem, whose solution is

$$\frac{u}{U_0}=1-erf\left(\frac{y}{2\sqrt{\nu t_0}}\right) \tag{5}$$

where U_0 is the velocity of the plate, ν is the kinematic viscosity, and t_0 is the time from the impulsive start. The correction u_{cor} is found from Eq. 5 by setting $U_0=-u(0,x)$ where $u(0,x)$ is the slip velocity along the wall at $t=0$. The slip velocity is induced by the vortex and its image. The time t_0 is chosen to be sufficiently small, so that the velocity and vorticity fields are not significantly altered except very near the wall. The corresponding vertical velocity component v is found from the continuity equation.

For the boundary conditions, which are only needed for the velocity, the no-slip and no-penetration conditions are applied at the wall while zero normal derivatives are specified at the top and outflow boundaries. The inflow boundary conditions consist of the Blasius profile plus a correction due to the vortex. Although the simulations were initialized with

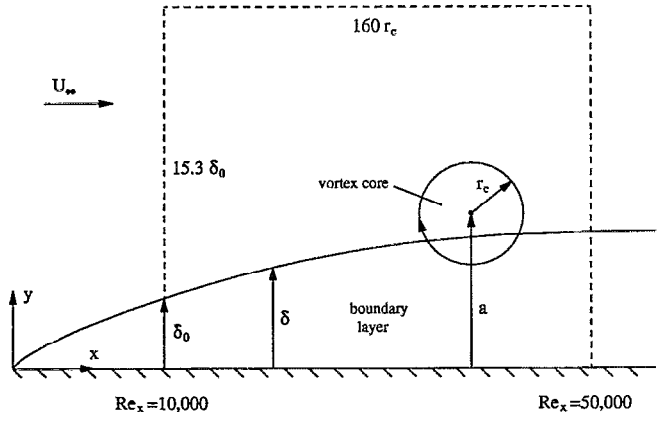

FIG. 3. The flow configuration.

TABLE I. Selected parameters of the three simulations.

	Case I	Case II	Case III
v_c/U_∞	0.50	0.50	1.80
a/r_c	3.20	3.20	3.00
a/δ	1.33	1.33	1.33
ω_{max}	+6944	−6944	−24883
Re_Γ	1097	1097	3952

the vortex at 20 core radii from the inflow boundary there is still a small velocity disturbance due to the vortex. For completeness this disturbance is accounted for by adding to the Blasius profile the velocity due to an inviscid vortex with the same strength and location as the physical vortex. The image vortex is also accounted for by this method. This correction is used initially and for all times.

III. RESULTS

The results for three different simulations are presented with relevant initial parameters shown in Table I and the general configuration shown in Fig. 3. The velocity scale is the freestream velocity while the length scale is $L_c=10^6\nu/U_\infty$. The vortex is characterized by its maximum tangential velocity, v_c, and its radius at this point, r_c (the core radius). The maximum initial vorticity of the vortex is ω_{max}. The height of the vortex above the wall is a, δ is the boundary-layer thickness, and Re_Γ is the Reynolds number based on the circulation of the vortex. Cases I and II are identical except for the sign of Γ. These cases concern a vortex with vorticity magnitude comparable to that of the boundary layer at the wall. The outflow boundary is at $x=0.05$ where $Re_x=50{,}000$. A grid of 1000×100 points was used, resulting in 13 grid points within the vortex core. Case III is similar to cases I and II but the vortex is much stronger. For case III the outflow boundary is at $x=0.03$ ($Re_x=30{,}000$) and a grid of 800×120 was used which results in 20 points in the core. For all cases, the Reynolds number based on x is $Re_x=10{,}000$ at the inflow. Initially the vortex has a diameter of approximately three quarters of the boundary-layer thickness and is positioned near the edge of the boundary layer. In no case does the vortex approach closer to the outflow boundary than 50 core radii.

The trajectories of the vortex center (defined as the point of maximum magnitude of vorticity) for all three cases are shown in Fig. 4. The vortex of case I (counterclockwise rotation) moves away from the wall, though it slows near the end of the simulation. In case II (clockwise rotation) the vortex moves toward the wall and also slows somewhat near the end of the simulation. In case III (clockwise rotation) the vortex initially approaches the wall and then rebounds. The present results are in general agreement with the experimental studies of Cerra and Smith[18] of a vortex ring impinging on a boundary layer. They noted that as the ring entered the boundary layer, the downstream end of the ring rebounded, while the upstream end continued closer to the surface. This resulted in a tilting of the ring. The counterclockwise vortex of case I, which rebounds, is analogous to the downstream end of the ring vortex of Cerra and Smith. Likewise, the

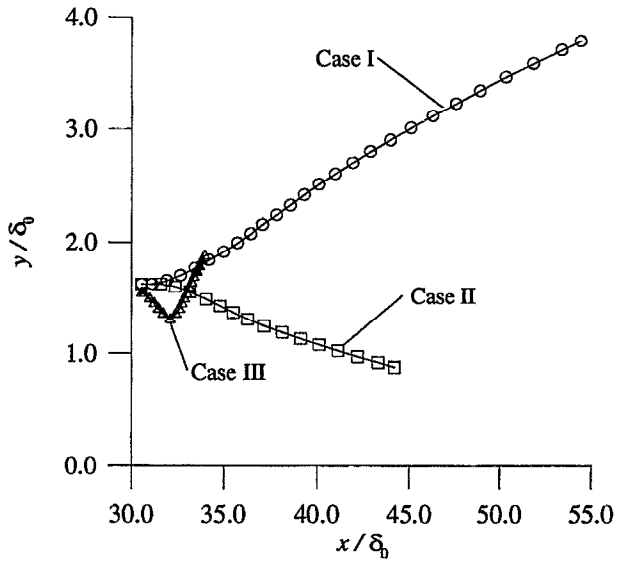

FIG. 4. The trajectories of the vortex center.

clockwise vortex of case II corresponds to the upstream end of the ring vortex. Cerra and Smith speculated that the tilting of the vortex ring was due to its interaction with the vorticity of the boundary layer. An examination of the vorticity distributions for the three cases of the present work supports this mechanism as the cause for the vortex trajectories.

Figure 5 shows the vorticity contours at different instants in time for case I. The vorticity increments between consecutive contour lines are fixed and are the same for each plot. Dotted lines represent positive vorticity while solid lines represent negative vorticity. The negative vorticity of the boundary layer is lifted away from the wall and wrapped around the vortex. This process is similar to the eruption phenomenon, yet the weak vortex generates no significant vorticity at the wall. The vortex primarily redistributes the vorticity of the boundary layer. While the uplifted region does not coalesce into a secondary vortex as observed in the eruption process, it is still a region of coherent vorticity which affects the vortex in an inviscid-like manner. The region of negative vorticity induces an upward motion to the vortex. The ascent of the vortex slows somewhat as it moves away from the wall since the region of negative vorticity weakens. Peace and Riley,[7] in their Navier-Stokes calculations, observed a slight rebounding of a vortex pair without the formation of a secondary vortex. Their simulations were at a lower Reynolds number ($Re_\Gamma = 100$) and contained no freestream.

The vorticity distribution suggests a possible three-dimensional mechanism for increased vortex decay. In a frame of reference moving with the vortex, the circulation around the core will decrease with radius for circuits enclosing the negative vorticity region. Vortices with non-monotonic radial distribution of circulation are susceptible to centrifugal instabilities according to the Rayleigh circulation criterion. It is possible that counter-rotating ring vortices could develop around the core of the primary vortex. The ring vortices would have centers lying along the axis of the primary vortex. While the primary vortex has vorticity in the axial direction only, the ring vortices would have only azimuthal vorticity. The ring vortices could increase the rate of decay of the primary vortex. Such a development can be seen

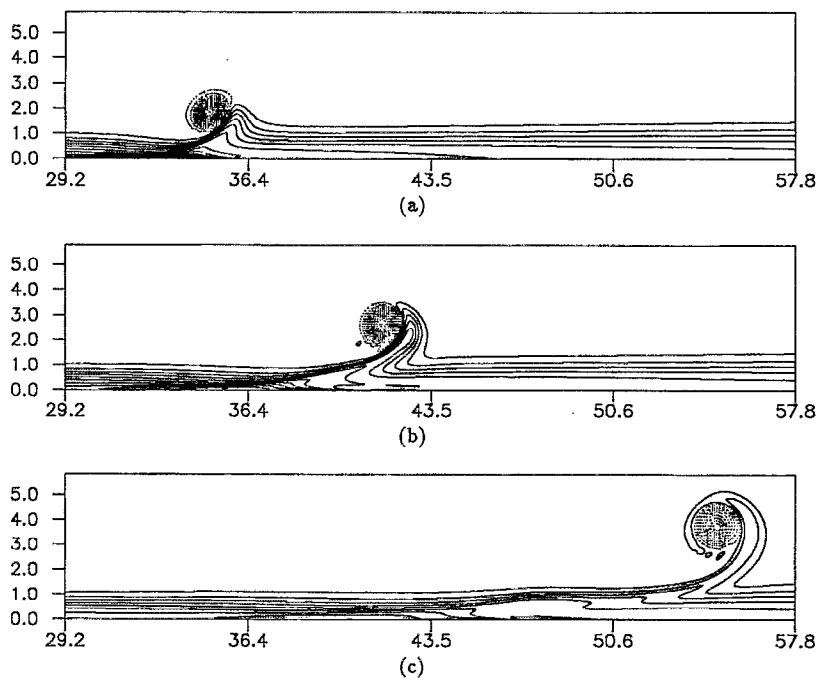

FIG. 5. Case I: The vorticity contours ranging from -9600 to 6300 with constant steps of 408. (a) $t=0.00194$, (b) $t=0.00492$, (c) $t=0.01101$. The dimensions are scaled by δ_0.

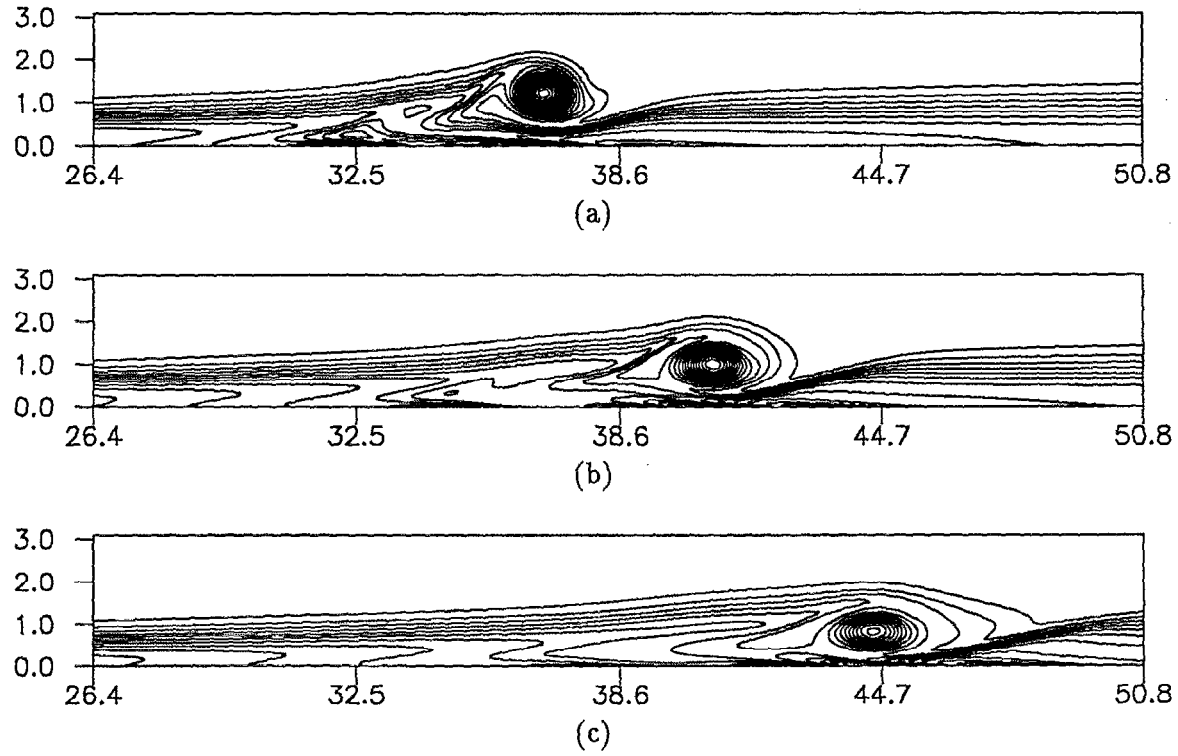

FIG. 6. Case II: The vorticity contours ranging from -6100 to 4600 with constant steps of 282. (a) $t=0.00393$, (b) $t=0.00690$, (c) $t=0.01019$. The dimensions are scaled by δ_0.

only in a three-dimensional simulation and has been observed for an isolated vortex.[19] Configurations of this type will be sought in future investigations.

The vorticity contours at various times for case II are shown in Fig. 6. Positive vorticity is created at the wall due to the vortex but it remains near the wall and does not erupt into the outer flow. A concentration of negative vorticity exists on the wall immediately upstream of the positive vorticity layer. In Figs. 6(b) and 6(c) this negative vorticity can be seen to move upstream relative to the vortex. The positive vorticity region corresponds to a small separation region caused by the adverse pressure gradient imposed by the vortex. This can be seen in Fig. 7 which shows the instantaneous streamlines. As the vortex convects it moves toward the wall, becoming distorted. This movement is due to the collection of boundary layer vorticity immediately upstream of the vortex. Thus, instead of an eruption and rebound, the vortex moves even closer to the wall. The convection velocity of the vortex slows down ($u=0.53$ at the end of the simulation) as the vortex moves into a region of lower velocity and the effect of the image vortex is stronger. It is also apparent that the vortex entrains essentially irrotational fluid into the boundary layer.

Our results indicate that vortices with the same sign as the vorticity of the boundary layer should have the tendency of moving closer to the wall. Turbulent eddies that comprise a turbulent boundary layer would therefore also tend to contain themselves within a layer next to the wall. This is a somewhat simplistic representation, because the vortices in a turbulent boundary layer are mostly three-dimensional in character.

Case III concerns a negative vortex with vorticity an order of magnitude larger than that of the boundary layer. The disparity in the strengths of the vorticity fields suggests that there would be little interaction between the vortex and boundary layer. However, this case highlights the eruption phenomenon. A time sequence of the vorticity contours is shown in Fig. 8. Dotted lines represent negative vorticity

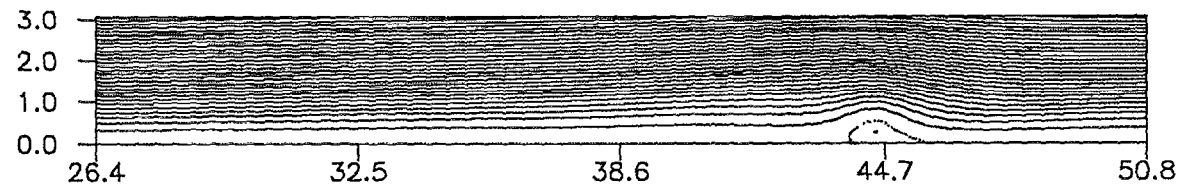

FIG. 7. Case II: The instantaneous streamlines viewed in a fixed reference frame. $t=0.01019$. The dimensions are scaled by δ_0.

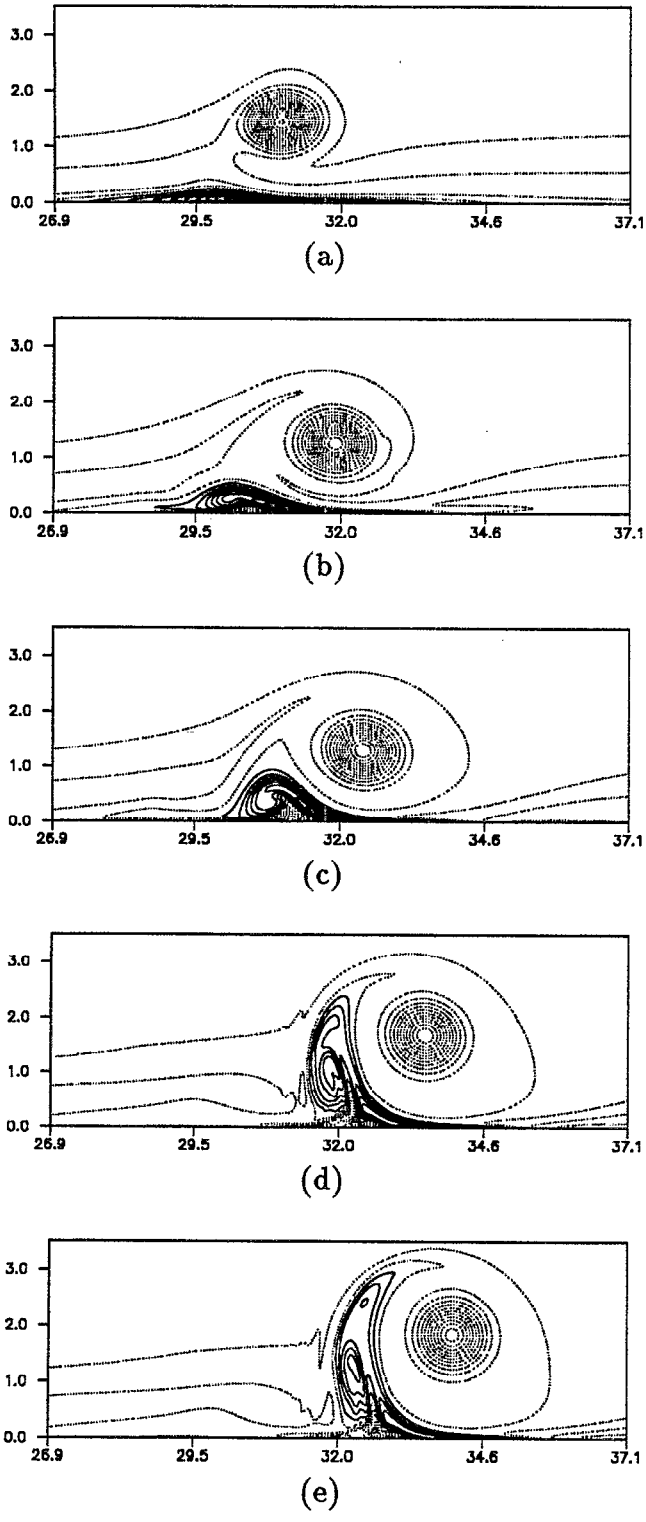

FIG. 8. Case III: The vorticity contours ranging from -24000 to 22000 with constant steps of 1586. (a) $t=0.00040$, (b) $t=0.00166$, (c) $t=0.00258$, (d) $t=0.00394$, (e) $t=0.00436$. The dimensions are scaled by δ_0.

while solid lines represent positive vorticity. The vortex creates a layer of strong positive vorticity next to the wall (Fig. 8(a)). This region looks similar to that produced by the weaker vortex of case II (see Fig. 6(a)). Upstream of the vortex the layer begins to thicken and lift away from the wall. Underneath the layer negative vorticity is generated at the wall due to the positive vorticity of the uplifted layer. A secondary vortex is beginning to form, as can be clearly seen in Fig. 9, which shows the instantaneous streamlines in a frame of reference moving with the vortex. The vorticity erupts into the outer region, where it interacts with the primary vortex in an inviscid-like fashion, causing the primary vortex to move outward. Initially the vortex moves downward, a response similar to that of case II. After eruption, however, the vortex moves upward, as expected.

As a check on the adequacy of the grid, case III was rerun for a grid refined by a factor of two thirds in both directions in the neighborhood of the vortex motion. An examination of the vorticity field revealed a slightly smoother distribution but no new structures. Another simulation using the original grid but with half the time step yielded results identical to case III. These simulations show that all relevant spatial and time scales are well resolved.

The decay of the peak vorticity (normalized by its initial value) for each case is shown in Fig. 10. Also shown is the decay of the peak vorticity for an isolated Oseen vortex. The negative vortices (cases II and III) closely match the isolated Oseen vortex, though there is a slight discrepancy near the end of the simulation for case II. In case II the vortex has become distorted as it approaches the wall, which might explain the slight deviation. The positive vortex, however, shows a larger deviation and a change in the decay rate near $t=0.005$. The simulation of case III was terminated after the eruption occurred.

Quantities along the wall, namely the friction and pressure coefficients, are also examined. Figure 11(a) shows the friction coefficient along the wall for case I at instants in time which correspond to those used in Fig. 5. Also shown is the friction coefficient as computed from the Blasius solution for flow over a flat plate. Away from the vortex the agreement with the Blasius solution is excellent. Initially the friction coefficient has a large maximum beneath the vortex. The peak decays quickly to moderate levels and moves upstream relative to the vortex. Elevated values of C_f remain for significant distances upstream of the vortex. The friction coefficient for case II, shown in Fig. 11(b), has a negative minimum, indicating the separation region below the vortex. The minimum C_f remains slightly downstream of the vortex center. The first peak is due to the concentration of negative vorticity at the wall upstream of the vortex and decays with time. Unlike case I, however, the friction coefficient has relatively constant values in the neighborhood of the vortex even though the vortex has decayed considerably. This is a result of the vortex moving closer to the wall. The coefficient of friction for case III (Fig. 11(c)) has the same general profile as in case II, though the magnitude is much larger. The large C_f is indicative of the negative vorticity generation under the uplifted vortical layer. Unlike case II, however, the peak positive value of C_f is increasing with time until eruption, when it decreases quickly. The minimum as well weakens considerably and remains downstream of the vortex center.

The response of the pressure coefficient is similar to that of the friction coefficient. The pressure coefficient for case I,

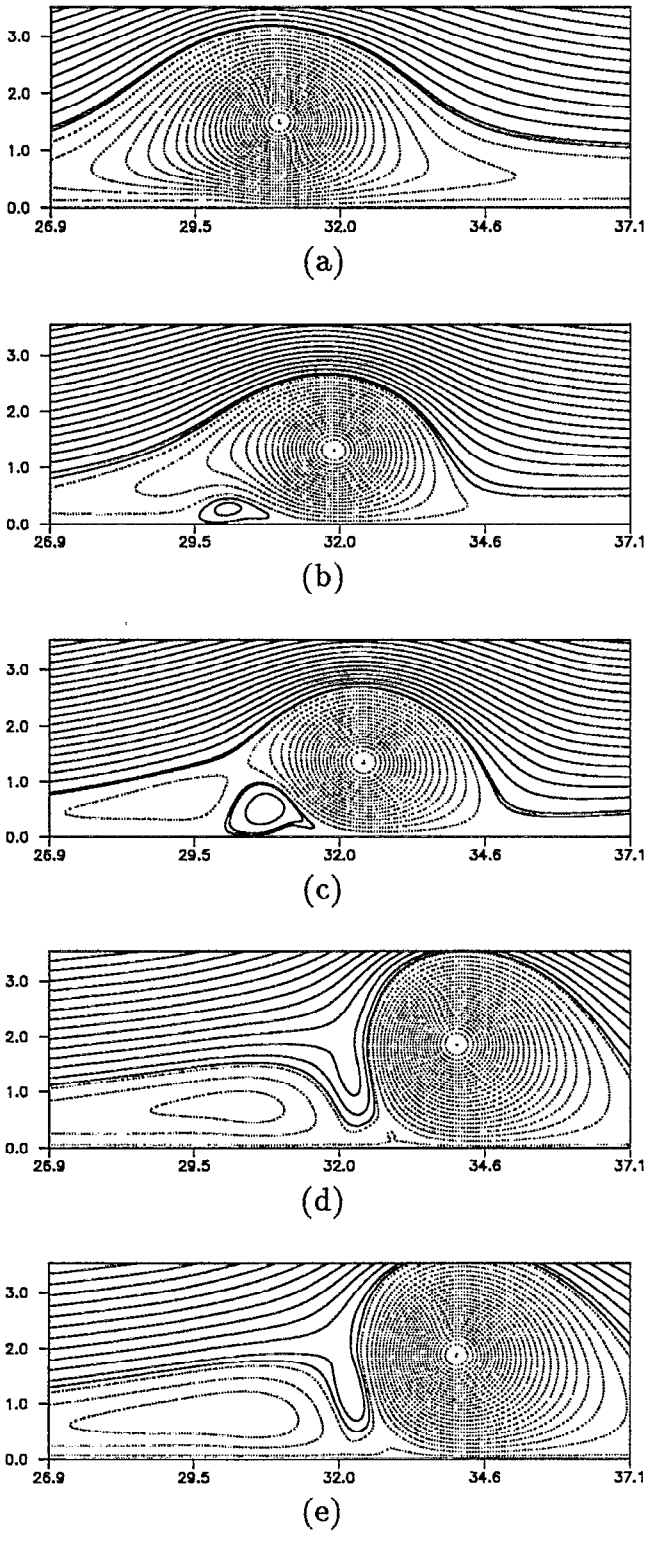

FIG. 9. Case III: The instantaneous streamlines viewed in a moving reference frame. (a) $t=0.00040$, (b) $t=0.00166$, (c) $t=0.00258$, (d) $t=0.00394$, (e) $t=0.00436$. The dimensions are scaled by δ_0.

shown in Fig. 12(a), shows the same trends as the friction coefficient. For case II (Fig. 12(b)), the pressure has a minimum beneath the vortex. There is also a small disturbance which corresponds to the negative vorticity region upstream

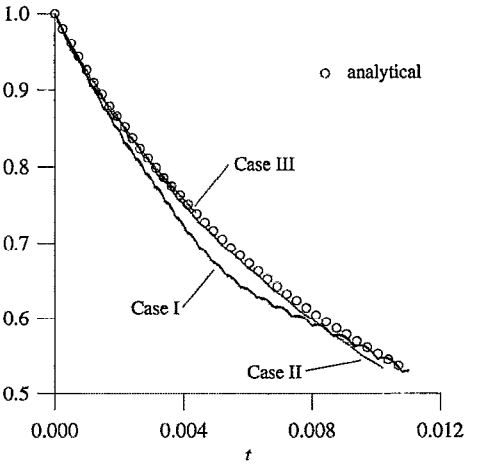

FIG. 10. The decay of the peak vorticity compared to an isolated Oseen vortex.

of the vortex. In addition, there is a rather large overshoot in the pressure downstream of the vortex. In case III (Fig. 12(c)), the minimum C_p is also beneath the vortex. This value abruptly increases after eruption. The region under the secondary vortex also experiences an increase in pressure.

Velocity profiles for case III are shown in Fig. 13. The velocities on two vertical lines, one through the primary vortex and one through the secondary vortex, are shown for two different times. These times correspond to those used in Figs. 8(c) and 8(d). The peak u velocity of the primary vortex is approximately $2U_\infty$ while it is approximately U_∞ for the secondary vortex. Both profiles change very abruptly near the wall. At $t=0.00394$ the secondary vortex has moved upward (Fig. 8(d)) and the u profile of the secondary vortex has become strictly positive. The vertical velocity (Fig. 13(b)) for the secondary vortex remains strong, approximately $0.4U_\infty$ for the maximum. Its peak near the wall, however, has decayed considerably. The primary vortex shows no qualitative change, though it has decayed somewhat.

IV. CONCLUSIONS

Numerical solutions to the incompressible Navier-Stokes equations have been calculated for various spanwise vortices in close proximity to a boundary layer. For a boundary layer containing negative vorticity, a sufficiently strong negative (clockwise) vortex induces an eruption of opposite sense vorticity and the generation of a secondary vortex which induces the rebound of the primary vortex. The general nature of the response is the same as that observed for vortex rings or pairs impinging on a wall. However, for weaker vortices in which the vorticity of the vortex and boundary layer are the same order the response is much different. Instead of the vortex creating a strong eruption, it mainly redistributes the vorticity of the boundary layer, causing the primary vortex to move closer to the wall instead of rebounding. The response of the boundary layer to a positive (counterclockwise) vortex resembles the eruption process in that negative vorticity is uplifted, causing the primary vortex to rebound. It may be argued that this negative vorticity is a secondary vortex but it

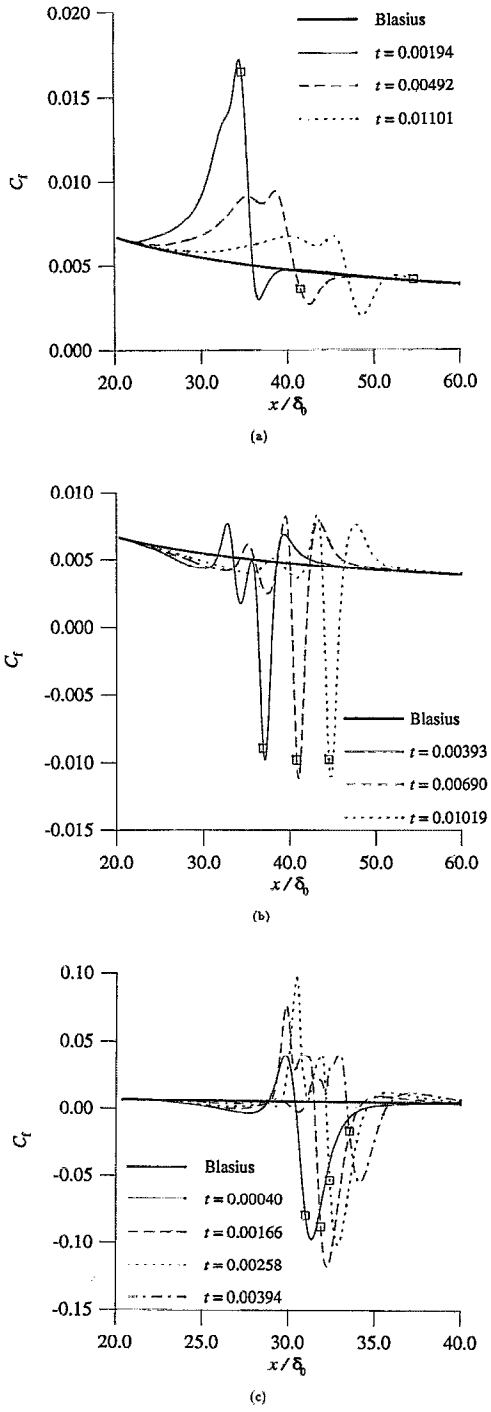

FIG. 11. The friction coefficient at various instants in time. (a) case I, (b) case II, (c) case III. The symbols represent the location of the vortex center.

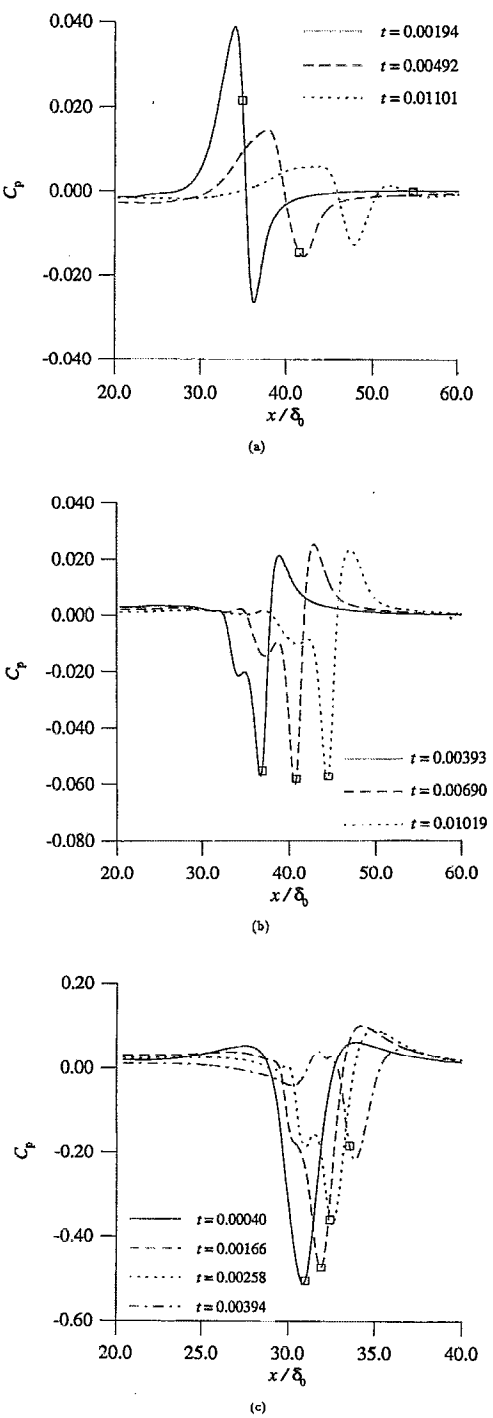

FIG. 12. The pressure coefficient along the wall at various instants in time. (a) case I, (b) case II, (c) case III. The symbols represent the location of the vortex center.

did not form by the sudden eruption of wall vorticity. It is an accumulation of boundary layer vorticity downstream of the vortex.

The weaker negative vortex produces positive vorticity and a small, persistent separation region which remains at the wall under the vortex. This vorticity layer does not erupt into the outer flow. Nevertheless, the boundary layer vorticity is redistributed, inducing a downward motion to the vortex. As the vortex moves closer to the wall, it generates stronger vorticity through the no-slip condition. The ultimate fate of the vortex, whether it decays or induces an eruption, is dependent upon the Reynolds number. Previous experimental results for turbulent flow indicate that a negative vortex embedded within the boundary layer is quickly destroyed. The current study for laminar flow showed no appreciable change in the rate of decay of the vortex. Indeed, this was true for all cases considered. It should be noted, however, that the re-

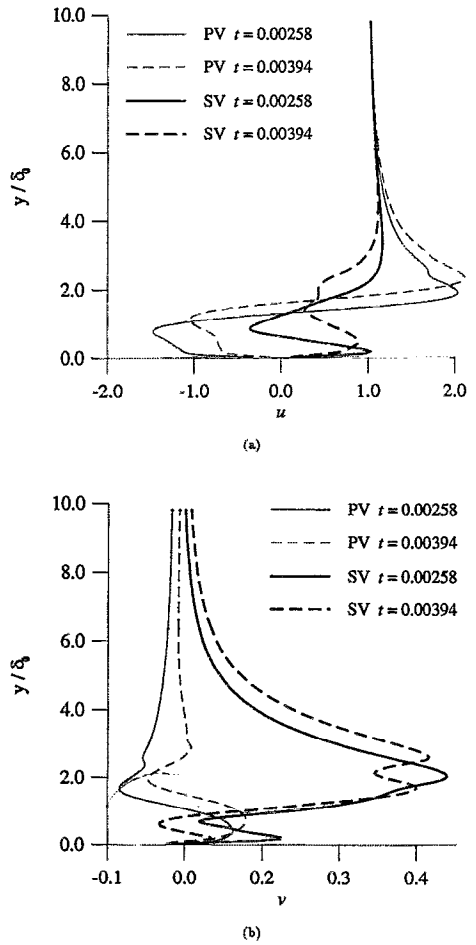

FIG. 13. The velocity on lines through the primary vortex (PV) and secondary vortex (SV) at two instants in time. (a) Streamwise velocity, (b) vertical velocity.

sponse of the system cannot be accurately predicted by methods that assume the vortex remains at a constant height above the wall. In addition, the vortices strongly affect the pressure and shear on the wall for a distance of several core diameters, especially upstream of the vortex.

The results of the current study exhibit features similar to previous studies of vortex/wall interaction as well as new features due to vortex/boundary-layer interaction. In addition to the familiar rebound phenomenon, the interaction between the vortex and the vorticity of the boundary layer affects not only the trajectory of the vortex but also the friction and pressure signatures along the wall. The present method can be extended to include three-dimensional effects or turbulence. These additions, as well as higher Reynolds number studies, would certainly improve the current understanding of vortex/boundary-layer interactions.

ACKNOWLEDGMENTS

This work is supported by the Office of Naval Research under Grant No. N00014-930264. The second author is also supported by ONR, Grant No. N00014-92-J-4087.

[1]C. Koromilas and D. P. Telionis, "Unsteady laminar separation—an experimental study," J. Fluid Mech. **97**, 347 (1980).
[2]E. R. Booth, Jr. and Y. C. Yu, "Two-dimensional blade-vortex visualization investigation," AIAA J. **24**, 1468 (1986).
[3]D. K. Tafti and S. P. Vanka, "A numerical study of flow separation and reattachment on a blunt plate," Phys. Fluids A **3**, 1749 (1991).
[4]S. K. Robinson, "Coherent motions in the turbulent boundary layer," Annu. Rev. Fluid Mech. **23**, 601 (1991).
[5]T. L. Doligalski, C. R. Smith, and J. D. A. Walker, "Vortex interactions with walls," Annu. Rev. Fluid Mech. **26**, 573 (1994).
[6]J. K. Harvey and F. J. Perry, "Flowfield produced by trailing vortices in the vicinity of the ground," AIAA J. **9**, 1659 (1971).
[7]A. J. Peace and N. Riley, "A viscous vortex pair in ground effect," J. Fluid Mech. **129**, 409 (1983).
[8]P. Orlandi, "Vortex dipole rebound from a wall," Phys. Fluids A **2**, 1429 (1990).
[9]P. Orlandi and R. Verzicco, "Vortex rings impinging on walls: Axisymmetric and three-dimensional simulations," J. Fluid Mech. **256**, 615 (1993).
[10]U. Boldes and J. C. Ferreri, "Behavior of vortex rings in the vicinity of a wall," Phys. Fluids **16**, 2005 (1973).
[11]J. D. A. Walker, C. R. Smith, A. W. Cerra, and T. L. Doligalski, "The impact of a vortex ring on a wall," J. Fluid Mech. **181**, 99 (1987).
[12]N. Didden and C. M. Ho, "Unsteady separation in a boundary layer produced by an impinging jet," J. Fluid Mech. **160**, 235 (1985).
[13]C. F. Nelson, D. J. Koga, and J. K. Eaton, "Unsteady, separated flow behind an oscillating, two-dimensional spoiler," AIAA J. **28**, 845 (1990).
[14]F. Chuang and A. T. Conlisk, "The effect of interaction on the boundary layer induced by a convected rectilinear vortex," J. Fluid Mech. **200**, 337 (1989).
[15]V. J. Peridier, F. T. Smith, and J. D. A. Walker, "Vortex-induced boundary-layer separation. part 2. unsteady interacing boundary-layer theory," J. Fluid Mech. **232**, 133 (1991).
[16]J. Kim and P. Moin, "Application of a fractional-step method to incompressible Navier-Stokes equations," J. Comput. Phys. **59**, 308 (1985).
[17]H. Le and P. Moin, "An improvement of fractional-step methods for the incompressible Navier-Stokes equations," J. Comput. Phys. **92**, 369 (1991).
[18]A. W. Cerra and C. R. Smith, "Experimental observations of vortex ring interaction with the fluid adjacent to a surface," Report FM-4, Dept. of ME/Mech., Lehigh University, 1983.
[19]M. Sreedhar and S. Ragab, "Large-eddy simulation of a stationary longitudinal vortex," Phys. Fluids **6**, 2501 (1994).